

# A molecular dynamics simulation of the melting points and glass transition temperatures of myo- and neo-inositol

Stephen W. Watt

*Department of Chemistry, The Pfizer Institute for Pharmaceutical Materials Science, University of Cambridge, Lensfield Road, Cambridge CB2 1EW, United Kingdom*

James A. Chisholm

*The Pfizer Institute for Pharmaceutical Materials Science, Cambridge Crystallographic Database Centre, 12 Union Road, Cambridge CB2 1EZ, United Kingdom*

William Jones

*Department of Chemistry, The Pfizer Institute for Pharmaceutical Materials Science, University of Cambridge, Lensfield Road, Cambridge CB2 1EW, United Kingdom*

Sam Motherwell

*The Pfizer Institute for Pharmaceutical Materials Science, Cambridge Crystallographic Database Centre, 12 Union Road, Cambridge CB2 1EZ, United Kingdom*

(Received 23 December 2003; accepted 23 August 2004)

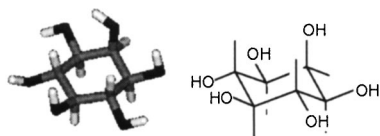
The heat of sublimation, density, melting point, and glass transition temperature are calculated for myo- and neo-inositol, using the condensed-phase optimized molecular potentials for atomistic simulation studies (COMPASS) [H. Sun, *J. Phys. Chem. B* **102**, 7338 (1998)] force field and molecular dynamics techniques. Our results show that the calculated heats of sublimation and density are very close to the experimental values for both compounds. Furthermore, our simulated melting temperatures for myo- and neo-inositol also compare very well to the experimentally obtained data. The glass transition temperatures for myo- and neo-inositol have been calculated to be ca. 494 K and ca. 518 K, respectively, and the shape of the volume versus temperature plots produced are typical for a glass transition. As a result, it is our view that the COMPASS force field suitably describes these two compounds in molecular simulations and that molecular dynamics techniques, combined with this force field, can be used to simulate the melt and glass transitions for such molecules. © 2004 American Institute of Physics. [DOI: 10.1063/1.1806792]

## I. INTRODUCTION

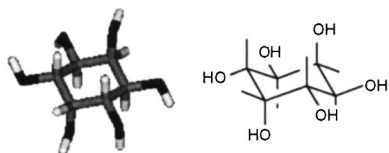
The introduction of high performance computers and novel force fields has allowed the accurate simulation of phase transitions in organic materials.<sup>1</sup> Over the last ten years a number of studies have attempted to simulate, usually by molecular dynamics techniques, the glass transition of amorphous polymers and saccharides. Han *et al.*<sup>2</sup> used molecular dynamics (MD) to simulate the glass transition of four polymers: *cis*-poly(1,3-butadiene), polyisobutylene, atactic polypropylene, and polystyrene. In this study, the authors distinguish between diffusive and vibrational motion and monitor the latter as a function of temperature to detect the glass transition. Tsige and Taylor<sup>3</sup> used diffusion coefficients, also obtained from MD, to calculate the glass transition temperature ( $T_g$ ) of poly(methyl methacrylate). With regard to saccharides, Caffarena and Grigera simulated the glass transition and crystalline melting of glucose<sup>4</sup> as well as the glass transition in a number of glucose hydrates.<sup>5</sup> For the melting point and glass transition temperature of glucose, they used a counting routine to monitor the extent of intermolecular hydrogen bonding as a function of temperature. The glass transition for these glucose hydrates was detected by monitoring the self-diffusion coefficient of water as a function of temperature. Conrad and de Pablo<sup>6</sup> studied the cryo-protectant properties of  $\alpha$ - $\alpha$ -trehalose by performing

MD simulations on aqueous solutions of the disaccharide. In this study, the density of the amorphous matrix was monitored as a function of temperature to detect  $T_g$ . Mazeau and Heoux<sup>7</sup> used MD techniques to study the structural differences between crystalline and amorphous cellulose. Amongst the properties calculated by the authors was the glass transition temperature for amorphous cellulose, determined from volume versus temperature plots. Finally, in 2002 Yoshioka *et al.*,<sup>8</sup> used molecular dynamics to predict the glass transition temperature of aqueous solutions of glucose. In this study, the authors monitored density as a function of temperature to detect the glass transition temperature. Although the densities calculated in this study were not validated against their experimentally determined counterparts, the density of 1.43 g cm<sup>-3</sup> calculated for pure amorphous  $\alpha$ -glucose seems to be consistent when compared to the experimental value of 1.56 g cm<sup>-3</sup> obtained for the crystal.

As part of a wider study, both experimental and computational, on saccharides, we have investigated two closely related molecules: myo- and neo-inositol. These two isomeric compounds (Fig. 1) differ in only one aspect of molecular configuration: myo-inositol has only one hydroxyl group in an axial position whereas neo-inositol has two. The resulting difference in melting point between these two compounds is, however, ca. 90 K,<sup>9,10</sup> a very large value consid-



Myo-inositol - melting point 498 K [9]



Neo-inositol - melting point 588 K [9]

FIG. 1. Three-dimensional molecular structures and the reported experimental melting points of myo- and neo-inositol.

ering the small difference between their molecular geometries.

Using myo- and neo-inositol, the work reported herein aims to use computer simulation methods to achieve the following objectives: (i) Validate a modeling methodology (including choice of force field) for glass transition studies, and (ii) simulate the glass transitions for myo- and neo-inositol.

With regard to (i), we have used the condensed-phase optimized molecular potentials for atomistic simulation studies (COMPASS) force field<sup>11</sup> to calculate energies using both MD and energy minimization techniques.<sup>12</sup> This generic force field has been shown to possess two key features important to the current study: (i) it successfully predicts a number of physical properties exhibited by carbohydrate compounds; and (ii) it is specifically parametrized for condensed phases.<sup>11</sup> In order to validate this force field for myo- and neo-inositol, a number of physical properties are calculated and compared with their experimentally obtained counterparts. The three physical properties to be calculated for force field and methodology validation purposes are as follows:

- (a) Heat of sublimation.
- (b) Density at 298 K.
- (c) Melting point.

Three of the studies previously mentioned<sup>4,5,8</sup> gauge the quality of the force field parameters according to how close the simulated glass transition  $T_g$  temperature matches the experimental value. Although these studies elegantly illustrate a number of useful points, it should be noted that comparing simulated  $T_g$  values with experimentally obtained glass transition temperatures may not be a satisfactory validation criterion. The molecular dynamics simulation techniques used by these investigators simulate heating rates in the picosecond to nanosecond time regime, whereas the experimental techniques used to determine  $T_g$  (usually by differential scanning calorimetry or dilatometry methods) in-

volve significantly slower heating rates (of the order of 10 °C/min). As the observed glass transition temperature varies according to how much relaxation a material has undergone<sup>13</sup> (which in turn depends on how long a material spends at a temperature high enough to allow structural change) it is unlikely that the simulated and experimentally obtained glass transition temperatures will agree precisely. This discrepancy has already been mentioned by various authors.<sup>2,3,6,7</sup>

Of the three physical properties that are calculated to validate the use of the COMPASS force field, simulating acceptable melting points for myo- and neo-inositol is probably the most challenging. Ferretti *et al.*<sup>14</sup> calculated the melting point for succinic anhydride to within 10 K of the literature value using molecular dynamics techniques. The authors first adapted the OPLS force field<sup>15</sup> to reproduce the density of this compound at 298 K along with its heat of sublimation energy. They then proceeded to calculate a melting point by monitoring the cell density as a function of temperature. The apparent agreement between the calculated and experimentally determined melting points using their approach for succinic anhydride might well be fortuitous in this case given the effects of superheating that must undoubtedly lead to a higher calculated melting point, as recognized by Morris and Song.<sup>16</sup> Indeed, Morris and Song, appear to have alleviated this problem by introducing liquid regions into their crystalline model. These regions accelerate the melting process and reduce superheating by effectively seeding the growth of the fluid phase around the melting temperature. The authors used NVE molecular dynamics to successfully simulate the melting transition of a Lennard-Jones system. To investigate these points further we report here three different approaches that we have used to simulate the melting point: one method that ignores any possible superheating effect (method 1); and two others (methods 2 and 3) that adopt a methodology similar to that proposed by Morris and Song.<sup>16</sup>

## II. METHODS

### A. Computer hardware and software

All calculations were performed on a dual processor Octane2 silicon graphics workstation running IRIX64 (release 6.5) system operating software. Limitations associated with the licensing of the modeling software, meant that all calculations could only be performed on a single processor (600 MHz). The OFF modules in the Cerius<sup>2</sup> (version 4.6) (Ref. 17) molecular modeling environment were used to perform all energy minimizations and molecular dynamics simulations, and the builder module (also incorporated in Cerius<sup>2</sup>) was used to expand unit cells into supercells. The crystallographic coordinates of both myo- and neo-inositol (see later also) were obtained from crystallographic structural database<sup>18</sup> searches using a windows based Hewlett Packard personal computer (1.7 GHz) running Conquest (version 1.5).<sup>19</sup> The results of these searches were displayed in Mercury (version 1.1.1).<sup>19</sup>

## B. General molecular dynamics methodology

The computer modeling carried out in this work involves numerous energy minimization steps (relaxation) and MD simulations. Minimization steps were performed using the COMPASS force field and the smart minimizer algorithm, available within Cerius<sup>2</sup>. Furthermore, these steps were carried out using the EWALD summation technique<sup>12</sup> to calculate the long-range electrostatic forces. MD simulations were performed using the Verlet-Verlag velocity integration algorithm<sup>12</sup> and a time step of 1 fs. The COMPASS force field<sup>11</sup> was used to calculate the energy during each dynamics run and the nonbonded (van der Waals and electrostatic) forces were truncated using direct-space cutoffs. The choice of cutoff for the main MD runs was made according to two selection criteria: (i) the energy calculated from single point calculations on the starting models closely matched the energy calculated using the more accurate (but much more computationally expensive) EWALD summation technique;<sup>12</sup> (ii) increasing or decreasing the cutoffs by up to 1.5 Å did not significantly change the energy values in (i). Due to the different molecular arrangements in the models used in this study, the distance at which the electrostatic contributions converge must be different. Thus, we should not be surprised in the following sections by the use of different directspace cutoffs to deal with the nonbonded interactions of different molecular arrangements (i.e., models of the same compound used in methods 1 and 2 in the following sections). It is also important to note that all the direct-space cutoffs used in this study are smaller than half the length of the shortest supercell dimension.

Temperature control was provided in each simulation by the Berendsen thermostat,<sup>20</sup> and pressure was controlled using the Parrinello-Rahman barostat.<sup>21</sup> Furthermore, each *N-P-T* simulation was performed under atmospheric pressure.

The investigations outlined in Secs. II F and II G, respectively, attempt to simulate the melt and glass transitions. For methods 1 and 2 in Secs. II F and II G, respectively, the supercell volume is plotted as a function of temperature and transitions are detected from specific characteristics exhibited by the resulting profiles. It is important to emphasize that separate molecular dynamics runs were performed at several temperatures over an increasing temperature range. Each simulation lasted for at least 100 ps and the initial conditions (atomic coordinates, velocities, and supercell volume) for subsequent higher temperature molecular dynamics runs were provided by the final conditions of the previous lower temperature run. The initial starting coordinates for the first simulation in each case were provided by their respective energy minimized models (preparation outlined in the following sections) and the initial velocities were assigned from a Boltzmann distribution at 300 K. In all simulations, the molecules were allowed to be fully flexible, unless otherwise stated, and equilibration was attained when the volume of each supercell leveled out and stabilized over a period of time. With regard to the latter, this occurred in each simulation within the first 80 ps of the run. The period subsequent to equilibration was used to calculate bulk properties such as density, supercell volume, and temperature.

The construction of pressure versus temperature diagrams (method 3) was carried out using solid-liquid coexistence models and the NVE (constant volume, energy) ensemble. During these simulations the systems evolve towards an equilibrium temperature and pressure, which, by definition, is the melting point at a particular pressure. Furthermore, some of the solid may also melt during these simulations if the initial temperature is higher than the melting point; however, if the temperature is lower the system may initially solidify before reaching equilibrium. During these processes either kinetic energy is converted into potential energy to reflect the latent heat absorbed on melting, or potential energy is converted to kinetic energy to reflect the required increase temperature for the system to be brought to equilibrium from the solid. The same conditions (i.e., time step, direct-space cutoff) were used here as in model 2. The NVE runs were adjudged to have equilibrated when temperature and pressure leveled out and stabilized over a period of time. Each model was found to have partially melted when both initial and final models were compared.

## C. Validation of the COMPASS force field for myo- and neo-inositol

### 1. Heat of sublimation ( $\Delta H_{\text{sub}}$ ) calculation

The internal energy  $U_{\text{cryst}}$  of the crystalline phase, a necessary parameter in the calculation of  $\Delta H_{\text{sub}}$ , was calculated as follows: unit cells for myo-inositol and neo-inositol were obtained from the Cambridge structural database (CSD).<sup>18</sup> For each structure the cell was expanded to yield a supercell containing 128 molecules. Periodic boundary conditions were imposed on the supercell, and each molecule was allowed full conformational flexibility. The arrangement was then energy minimized and an energy minimum value  $U_{\text{cryst}}$  was obtained.

The internal energy of the gaseous phase  $U_{\text{gas}}$  was calculated as follows: a single molecule of myo- or neo-inositol was removed from the unit cell (obtained from the CSD) and then energy minimized. From this, an energy value  $U_{\text{gas}}$  was obtained.

Using a similar approach to that of Gavezzotti<sup>22</sup> and the expression below the values for  $U_{\text{cryst}}$ ,  $U_{\text{gas}}$ , and  $\Delta H_{\text{sub}}$  were calculated

$$\Delta H_{\text{sub}} = \Delta U - RT. \quad (1)$$

In this equation:  $\Delta H_{\text{sub}}$  is the enthalpy of sublimation ( $\text{J mol}^{-1}$ );  $\Delta U$  is the difference in internal energy between 1 mole of gaseous molecules and 1 mole of molecules in the crystalline arrangement (i.e.,  $U_{\text{gas}} - U_{\text{cryst}}/\text{J mol}^{-1}$ );  $R$  is the gas constant  $8.314 \text{ J K}^{-1} \text{ mol}^{-1}$ ;  $T$  is the absolute temperature (K).

### 2. Density calculation

The following protocol was used to calculate the density of both myo- and neo-inositol under atmospheric pressure at 298 K: a crystalline supercell containing 128 molecules was equilibrated under atmospheric pressure, at 298 K for 100 ps using *N-P-T* molecular dynamics.<sup>12</sup> Direct-space cutoff values of 9.5 and 12.5 Å were applied, respectively, to myo-

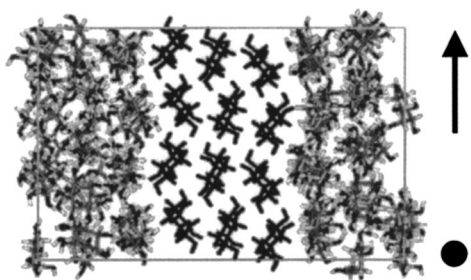


FIG. 2. Model used in method 2. Only model 2*a* for myo-inositol has been represented in this figure; however, a similar model has been produced for neo-inositol. The blackened species represent molecules that are constrained to remain in the crystalline configuration during high temperature NVT dynamics. The remaining regions represent the movable disordered regions that represent the liquid phase. The arrow and spot depict the vertical direction and the direction into the plane of the paper along in which the supercell is expanded by a factor of 2 to yield model 2*b*.

inositol and neo-inositol to truncate the nonbonded energy calculations. The density was calculated for each inositol from the final 20 ps of each simulation.

#### D. Preparation of melting point simulation models

As mentioned earlier, three approaches were used to simulate the melting points of each compound, i.e., methods 1, 2, and 3. Starting models for method 1 were prepared for MD using the following procedure: unit cells<sup>18</sup> of both myo-inositol and neo-inositol were obtained from the CSD and then expanded into separate supercells containing 128 molecules. The positions of the molecules were then relaxed to yield an energy minimized structure.

With regard to method 2, two slightly different supercells were constructed for each inositol, i.e., model 2*a* and model 2*b*. Model 2*a* was built using the starting model constructed for method 1 by the following procedure: within an arbitrary selected central region of the method 1 model, the positions of ca. 33% of the molecules were constrained to remain fixed (blackened molecules, Fig. 2). The remaining molecules were left unconstrained and able to move (non-blackened species). Two molecules were then permanently erased from each movable region (four molecules in total were removed) to assist molecular movement and a molecular dynamics simulation was performed on the supercell under constant volume and temperature (NVT ensemble<sup>12</sup>) at 1200 K for 150 ps. (A direct-space cutoff of 8.5 Å was applied to both inositol models in order to truncate the nonbonded energy calculations.) To yield the final model 2*a* configuration, the final frame from this high temperature simulation was minimized, first with the central region constrained and then with all atoms allowed to move. The construction of model 2*b*, on the other hand, followed a simpler procedure in comparison to model 2*a*. This particular supercell was constructed by expanding a previously prepared model 2*a* into a larger supercell containing 496 molecules. The expansion was made along the directions outlined in Fig. 2. Following the enlargement, the whole arrangement was energy minimized.

Finally, with regard to the starting models used in method 3 for both inositols, these were assemblies of the model 2*a* configuration described above.

#### E. Preparation of amorphous models of myo- and neo-inositol

A supercell was prepared by the procedure already outlined in Sec. II C 1. Four randomly chosen molecules were then permanently removed to assist molecular movement in the later MD simulations. The remaining molecules of this supercell were then manually repositioned within the supercell boundaries, using the tools available in Cerius<sup>2</sup>, to yield a disordered structure. This method of disordering the molecules ensured a completely random array of molecules. To prevent artificial close contacts occurring between these disordered molecules, the amorphous supercell was minimized and a NVT dynamics simulation was carried out at 400 and 500 K, for myo- and neo-inositol, respectively. The temperatures were chosen to avoid significant conformational change within the molecules. The last frame of this trajectory file was selected and the model energy minimized.

The above preparation method, to our knowledge, has not been attempted previously for the construction of amorphous models. We emphasize that the preparation attempts to create a truly random array of 124 molecules with no obvious short-range crystalline order. A future publication examining the microstructure of amorphous models of myo-inositol as a function of preparation method will show there to be little variation in the glass transition temperature when the method of preparation is varied.

#### F. Melting point simulation methodology

##### 1. Method 1

Independent molecular dynamics simulations were performed in 100 K steps between 300 K and 1200 K to equilibrate supercells of myo- and neo-inositol in the model 1 configuration.

The *N-P-T* ensemble was used for each simulation and direct-space cutoffs of 9.5 Å and 12.5 Å were employed, respectively, to truncate the nonbonded interactions of myo- and neo-inositol.

##### 2. Method 2

As mentioned in the introduction, the current work embodies a method similar to the one employed by Morris and Song in which they, *inter alia*, calculate the melting point of an atom based Lennard-Jones system. However, the methodology presented here differs slightly to Morris and Song in that the *N-P-T* ensemble is employed (as opposed to the NVE ensemble). By using the constant pressure-temperature ensemble macroscopic profiles such as volume versus temperature plots can be compared to experimentally obtained profiles to ensure that the melt transition is indeed being simulated correctly. We feel that this is an important validation requirement.

The constant pressure-temperature simulations are carried out on the coexistence models prepared in Sec. II C (model 2*a* and 2*b*). In each case, direct-space cutoffs of 10.3

and 9.45 Å for myo-inositol and neo-inositol, respectively, were used to truncate the nonbonded interaction calculations. These cutoffs were chosen according to criteria (i) and (ii) outlined in Sec. II B.

For both compounds, each molecule was again allowed to be fully flexible and simulations were performed under atmospheric pressure. For models 2*a*, both were equilibrated for 100 ps at: 300 K, 350 K, 400 K, 450 K, 500 K, 550 K, 600 K, 650 K, and 700 K. For models 2*b*: myo-inositol was equilibrated at 490 K, 500 K, 510 K, 520 K, and 530 K for 200 ps; neo-inositol was equilibrated for the same length of time at 560 K, 570 K, 580 K, 600 K, and 620 K. The temperature regions explored for model 2*b* were specifically selected to encapsulate the literature melting point values of both inositols and to reduce the number of lengthy MD runs required. The method of temperature increase between increments has been explained in Sec. II B.

### 3. Method 3

Method 3 resembles more closely the approach of Morris and Song.<sup>16</sup> Starting models of myo- and neo-inositol were primed for the NVE simulations by, respectively, equilibrating each at 505 and 575 K under atmospheric pressure for 20 ps using the *N-P-T* ensemble. The final conditions of these runs were used as the initial starting conditions for NVE simulations. These constant volume-energy molecular dynamics runs were initially carried out for 20 ps during which time the velocities were adjusted to the temperatures employed in the prior *N-P-T* run using the velocity scaling method.<sup>12</sup> (Employing this crude method of temperature control helped speed up equilibration.) Subsequent to this, the velocity scaling was removed and the simulation was continued for a further 80 ps during which time pressure and temperature was found to have equilibrated. Temperature and pressures were calculated over the final 20 ps of this latter MD run. The procedure was repeated several times using separate starting models; however, in each separate run the volume of the supercell was increased slightly following the priming step. From these simulations, the melting point of each inositol was plotted as a function of pressure and from the resulting graphs converged melting temperatures for both compounds at atmospheric pressure were obtained.

### G. Molecular dynamics simulation of the glass transition

For myo-inositol, an amorphous supercell was equilibrated for 100 ps in separate MD runs between 300 and 600 K (50 K intervals), and for neo-inositol the same simulation time was employed; however, equilibrations were made between 300 and 700 K (50 K intervals). All simulations were performed under atmospheric pressure and direct-space cutoffs of 10.3 and 9.45 Å were employed to truncate the nonbonded contributions for the myo- and neo-inositol models, respectively.

TABLE I. Experimental and calculated values for the heat of sublimation  $\Delta H_{\text{sub}}$  and densities of myo- and neo-inositol.

	$\Delta H_{\text{sub}}$ (kJ mol <sup>-1</sup> )		Density (g cm <sup>-3</sup> )	
	Expt.	Calc.	Expt.	Calc.
Myo-inositol	161	159	1.570	1.575
Neo-inositol	...	181	1.694	1.676

## III. RESULTS AND DISCUSSION

### A. Validation of the COMPASS force field

Table I displays the heat of sublimation  $\Delta H_{\text{sub}}$  and the density calculated for myo- and neo-inositol. The agreement between the calculated and experimentally determined values of myo-inositol is very good, which indicates that the COMPASS force field adequately describes these two compounds in energy calculations. Although an experimental value for  $\Delta H_{\text{sub}}$  is not available for neo-inositol, the calculated value is higher than that of myo-inositol, which one would expect for a material possessing a higher melting point.

### B. Melting point simulations

Figures 3 and 4 display the volume versus temperature plots calculated for methods 1 and 2 of myo- and neo-inositol, respectively. In each graph, the melting point is apparent from the characteristic sharp increase in volume that describes the first-order nature of the melt transition.<sup>23-25</sup> The melting points calculated using the method 1 approach are 675 K and 1120 K for myo- and neo-inositol, respectively [Figs. 3(a) and 4(a) respectively]. Therefore, for both myo- and neo-inositol, method 1 yields a melting point that is significantly higher than their literature values of 498 K and 588 K, respectively. Using model 2*a*, on the other hand, method 2 appears to be successful in reducing the simulated melting points of method 1 and yields a melting point of ca. 562 K for myo-inositol and ca. 660 K for neo-inositol –64 K and 72 K higher than the experimental values, respectively. Increasing the size of the model 2*a* supercell to give model 2*b* further improves these estimates. For example, model 2*b* yielded melting points for myo- and neo-inositol of ca. 505 K and 575 K, respectively, which are both within 15 K of their literature values. Switching from the *N-P-T* ensemble to the NVE ensemble as described for method 3, refines these melting points even further. From Fig. 5 melting points of 490 K and 578 K are obtained, respectively, for myo- and neo-inositol. Furthermore, the positive slopes of the melting point lines shown in Fig. 5 are entirely consistent with the abrupt increase in volume at the melting points of the two compounds (Figs. 3 and 4).

The results illustrate four very important points.

(i) Using an approach that does not account for superheating (method 1) can yield melting temperatures well above literature values.

(ii) Introducing liquid regions into the crystalline models (model 2*a*) alleviates superheating effects.

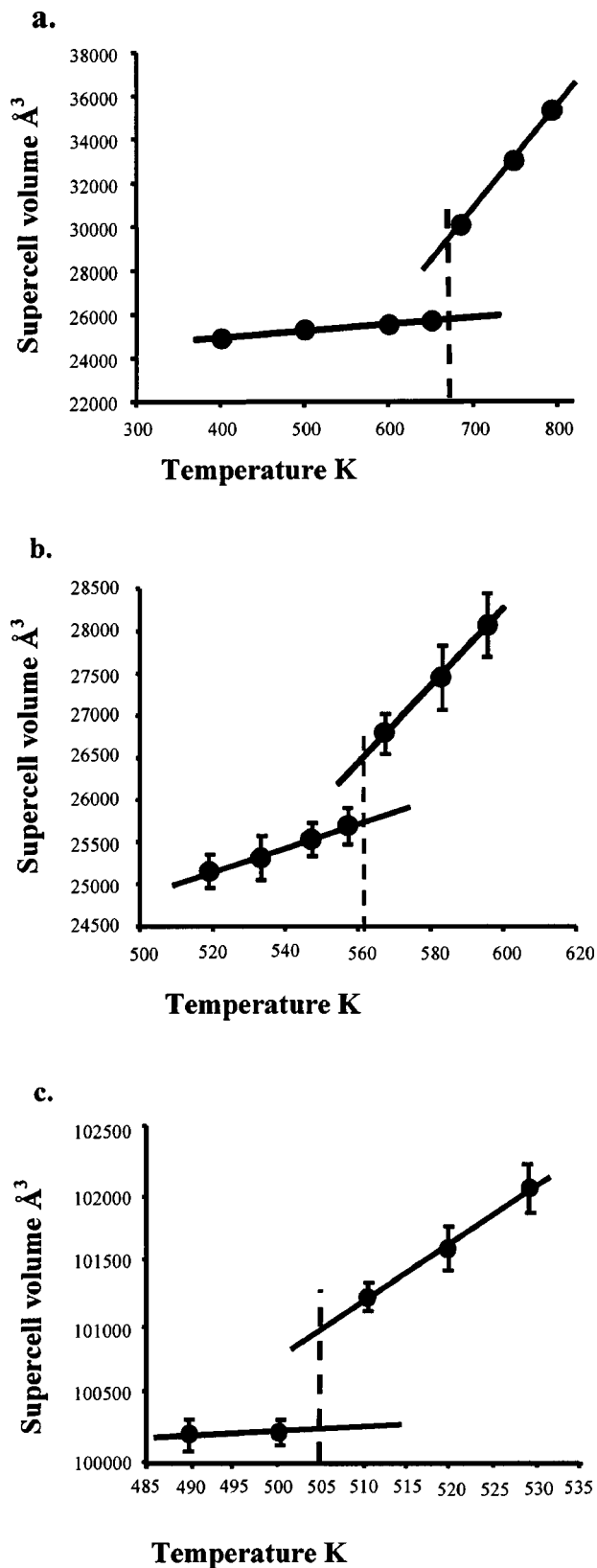


FIG. 3. (a) Plot of supercell volume vs temperature for myo-inositol using method 1. The broken vertical line displays the melting temperature, which has been estimated at 675 K. The error bands for each point are too small for display but range from  $\pm 120 \text{\AA}^3$  to  $\pm 230 \text{\AA}^3$ . (b) Supercell volume vs temperature plot for myo-inositol using model 2a and method 2. The broken vertical line displays the melting temperature, which has been estimated at 562 K. (c) Supercell volume vs temperature plot for myo-inositol using model 2b and method 2. Again, the broken vertical line displays the melting temperature, which has been estimated at 505 K.

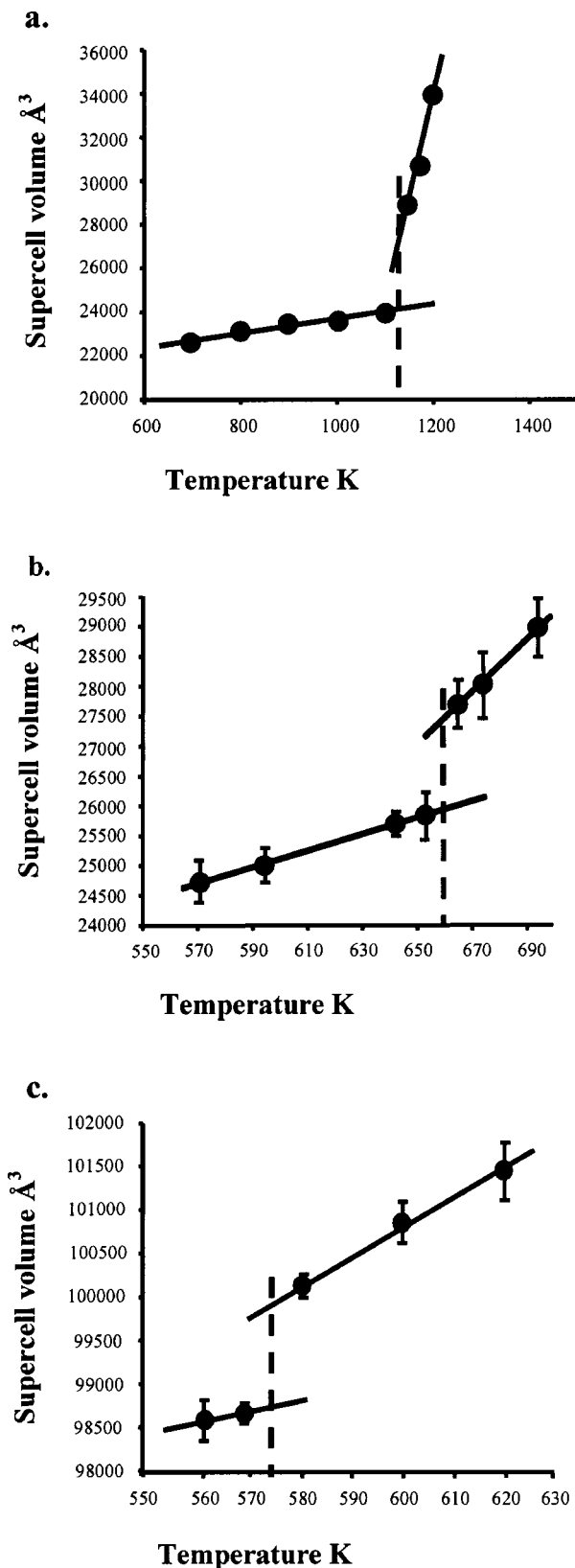


FIG. 4. (a) Plot of supercell volume vs temperature for neo-inositol using method 1. The broken vertical line displays the melting temperature, which has been estimated at 1120 K. The error bands for each point are too small for display but range from  $\pm 105 \text{\AA}^3$  to  $\pm 370 \text{\AA}^3$ . (b) Supercell volume vs temperature plot for neo-inositol using model 2a and method 2. The broken vertical line displays the melting temperature, which has been estimated at 660 K. (c) Supercell volume vs temperature plot for neo-inositol using model 2b and method 2. Again, the broken vertical line displays the melting temperature, which has been estimated at 575 K.

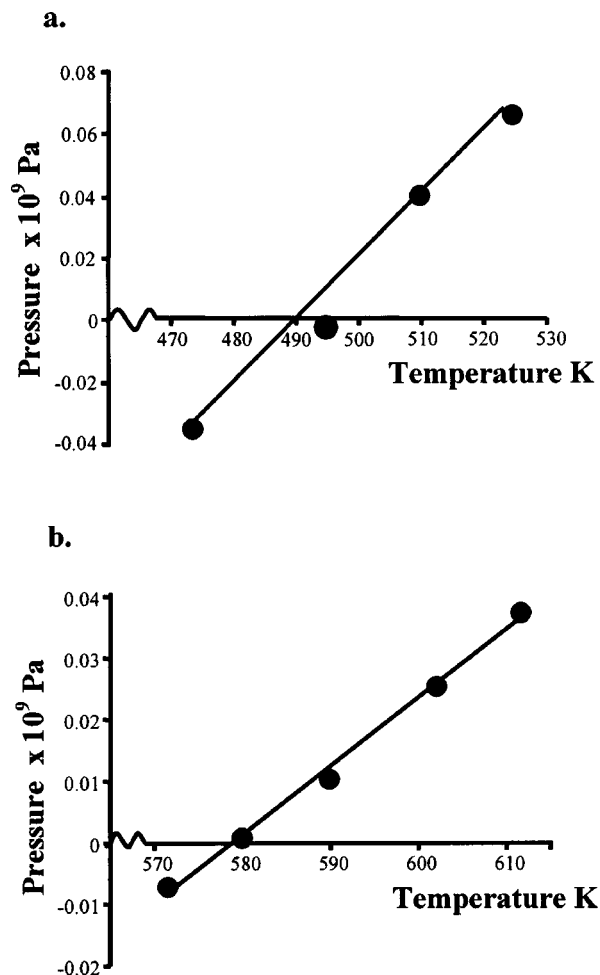


FIG. 5. Plot of melting point of myo- and neo-inositol as a function of pressure (method 3). (a) represents the calculated melting point line for myo-inositol and (b) represents the calculated melting point line for neo-inositol. The melting points at atmospheric pressure for myo- and neo-inositol have been calculated to be 490 K and 578 K, respectively.

(iii) Increasing the size of the coexistence cell and increasing the length of simulation time, can reduce superheating even further (model *2b*).

(iv) Switching from the constant pressure-temperature ensemble to the constant volume-energy ensemble eliminates superheating effects and provides precise and accurate melting points for both compounds.

With regard to (i), comparing the melting temperatures obtained from method 1 with experimentally obtained values, it is apparent that the short time scale of these molecular dynamics simulations is not long enough to observe, at lower temperatures, the nucleation and growth of the melt. As a result, the system is superheated to higher temperatures until the molecules possess sufficient momentum to surmount the energy barriers associated with the disordering of the crystalline configuration.<sup>16</sup> With regard to (ii), superheating is reduced since the starting models used in method 2 (i.e., model *2a*) already possesses liquid regions, i.e., regions are already disordered, hence the energy barriers for melting are reduced.<sup>16</sup> Finally, point (iii) illustrates that increasing the number of molecules in the starting models of method 2 (i.e., model *2b*) accelerates the melting process and reduces su-

perheating effects even further. This finding is probably due to an increased number of sites in which melting can be initiated from. The main drawback of using models of comparable size to model *2b* is that a ca. 14-fold increase in computation time is required for each simulation, i.e., using model *2a*, 100 ps of the simulation took  $\approx 24$  h to perform, whereas using model *2b*, 200 ps of the simulation took ca. 14 days to perform. With regard to point (iv), superheating effects are eliminated with the introduction of method 3 and precise melting points are obtained. Furthermore, the accuracy of these melting points to the experimentally obtained values again validates the COMPASS force field for these two compounds. It is also worth noting that the effect of superheating with method 2 is small given the simulated melting point values obtained for method 2 and method 3.

From the three approaches described, the following question arises: which model best describes the melting transition? The answer to this question is not straightforward. Although method 3 provides precise and accurate melting points in the present case, it does not simulate the experimental conditions in which melting points are obtained and thus its usefulness is limited in microscopic studies. In contrast, method 2 does simulate experimental conditions more closely but is continually dogged by superheating effects. Thus, for studies aimed at providing a microscopic explanation for a particular melt transition performing two separate simulations might be appropriate: one that follows method 3 (to validate the force field); and one that follows method 2 (for microscopic studies).

### C. Glass transition simulations

Figure 6(a) displays the change in volume as a function of temperature for the amorphous model prepared for myo-inositol. Comparing this diagram with experimentally determined volume versus temperature curves generally observed for amorphous materials, it is immediately apparent that the molecular dynamics simulations are successful in producing a glass transition. The temperature of this glass transition is estimated to be ca. 494 K (see figure); however, no experimental value is available for comparison.

Figure 6(b) displays the volume versus temperature diagram for the amorphous model prepared for neo-inositol. Again, this diagram displays a typical volume versus temperature profile for an amorphous material. The temperature of the glass transition is estimated to be ca. 518 K; however, an experimental value is not available for comparison.

### D. Microscopic considerations

The number of hydrogen bonds per molecule exhibited by myo- and neo-inositol in the crystal phases of both compounds is an obvious starting point when rationalizing the different melt and glass transition temperatures. From the crystal structures of both myo- and neo-inositol, we find that both compounds possess 12 hydrogen bonds per molecule (either donating or accepting). In fact, from a CSD search on other inositols we find that L-chiro-,<sup>26</sup> muco-,<sup>26</sup> and epi-inositol<sup>26</sup> also possess 12 hydrogen bonds per molecule. Furthermore, there appears to be no obvious pattern from the

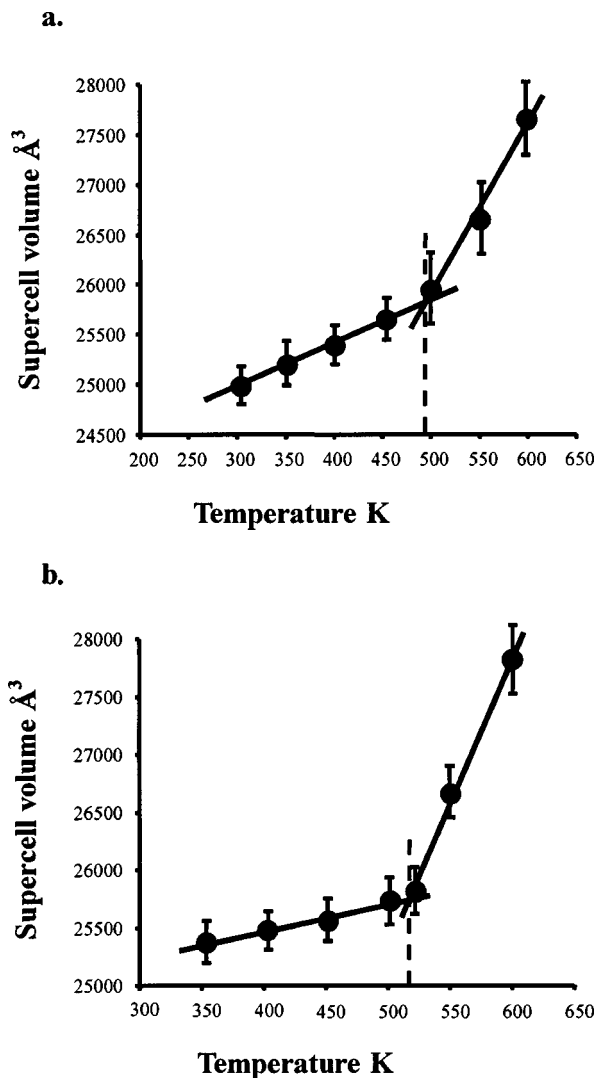


FIG. 6. (a) Supercell volume vs temperature plot for amorphous model of myo-inositol. The broken vertical line displays the glass transition temperature, which has been estimated at 494 K. (b) Supercell volume vs temperature plot for amorphous model of neo-inositol. The broken vertical line displays the glass transition temperature, which has been estimated at 518 K.

hydrogen bonding networks to indicate why myo- and neo-inositol melt at such vastly different temperatures in both the crystal and amorphous models. Our initial findings point towards differences in molecular packing of these molecules. For example, due primarily to the positions of axial hydroxyl groups on the molecules of these inositols, molecular packing in neo-inositol appears to be more efficient (compare densities in Table I). Thus, our preliminary examinations of the simulations presented in the current study indicate that the molecules of myo-inositol break up at a lower temperature simply due to this difference in packing, i.e., molecules of myo-inositol are not as efficiently locked into the crystalline configuration as their neo-inositol counterparts. Our studies are still ongoing in this area and involve quantum chemical techniques to investigate the possibility of variations in cooperative effects in the hydrogen bonding patterns exhibited in these two crystal structures.

## E. Evaluation of methodology and protocols

### 1. Direct-space cutoffs

The use of direct-space cutoffs can be a crude method of truncating the long-range electrostatic contributions and can lead to inaccuracies in a simulation.<sup>12</sup> On the other hand, Sun<sup>11</sup> noted that using the COMPASS force field with a direct-space cutoff to predict the density of a large number of liquids did not have a significant effect on MD simulations when compared to the highly accurate EWALD summation method. Sun<sup>11</sup> also reported that switching from the EWALD summation method to a direct-space cutoff of 10.5 Å decreased computation time by a factor of 20. In order to extend Sun's conclusions to our present systems, the following control test was performed on model 2a of myo-inositol: a number of separate MD simulations were carried out, as described in Sec. II F 2, at 560 K and 570 K using direct-space cutoffs of 8.0 to 11 Å (at 0.5 Å increments). The two temperatures chosen for this control test are significant since at 560 K the coexistence model of myo-inositol is crystalline and at 570 K it is molten liquid (Fig. 3). Therefore, if the simulated melting point is sensitive to the direct-space cutoff, then a significantly different volume is expected to be calculated at these temperatures, i.e., a higher melting point would be indicated by a lower volume for the 570 K simulation (to reflect the existing crystalline arrangement) and a lower melting point would be indicated by a larger volume for the 560 K run (to reflect the fluid molten state). As a further check at these two temperatures, the enthalpy difference between the two models at 560 and 570 K was calculated for each cutoff in these separate MD simulations.

Our results indicate that the supercell volume calculated at these particular temperatures does not vary significantly when the direct-space cutoff is changed from 8.0 to 11.5 Å, which suggests that the melting point also does not vary. Furthermore, the enthalpy difference calculated between the high (570 K) and low-temperature (560 K) molecular dynamics runs for each cutoff does not vary significantly (i.e., 8.0 Å = 54.34 kJ mol<sup>-1</sup>; 8.5 Å = 53.01 kJ mol<sup>-1</sup>; 9.0 Å = 52.96 kJ mol<sup>-1</sup>; 9.5 Å = 55.30 kJ mol<sup>-1</sup>; 10.0 Å = 53.85 kJ mol<sup>-1</sup>; 10.5 Å = 56.13 kJ mol<sup>-1</sup>; 11.0 Å = 53.24 kJ mol<sup>-1</sup>). Thus, it appears that the results described in this publication are not significantly affected by the direct-space cutoffs used in each instance.

Our attempts to use the EWALD summation method to deal with the long-range nonbonded interactions were not successful. Although this technique is the most desirable technique to use, it took ca. 72 h of computation time to perform 25 ps of the simulation. The former was deemed too long for the study in hand and the latter insufficient simulation time for the models to fully equilibrate. Thus an accurate supercell volume could not be determined from these tests. In comparison, using a direct-space cutoff to truncate long-range nonbonded interactions, 100 ps of each simulation was complete within 36 h.

## 2. Simulation time versus glass transition temperature

It is plausible that increasing the length of time that the amorphous models of myo- and neo-inositol spend at each temperature will affect the predicted glass transition temperature. Thus, in order to investigate how the glass transition temperature varies as a function of simulation time, the molecular dynamics simulations performed for 100 ps on amorphous models of myo-inositol were repeated at 400, 450, 500, 550, and 600 K, for 200 ps. Again, the initial conditions for each run were provided by the final conditions of the previous run.

The results have indicated that no deviation occurs from the plots outlined in Fig. 6 when the simulation time is increased from 100 to 200 ps. Furthermore, the volume calculated for this model also does not vary as a result of the increased simulation time. Again, it is worth noting that increasing the simulation time in this instance increased the cost in terms of time and computation, i.e., each individual simulation run at the temperatures listed above, took  $\approx 72$  h to complete.

## IV. CONCLUDING REMARKS

Using the COMPASS force field with direct-space cutoffs, the heat of sublimation and density of myo- and neo-inositol have been successfully calculated. Also using the COMPASS force field, the melt transition temperatures for myo- and neo-inositol have been simulated at atmospheric pressure using two different approaches (method 1 and method 2). Comparing the results from these simulations, the effect of superheating has been demonstrated. Furthermore, the results also show that the incorporation of liquid regions into the models used in these simulations alleviate these superheating effects. Further still, the study shows that the size of these coexistence models is critical in determining how much these superheating effects are reduced. Converged melting points of both myo- and neo-inositol have been calculated from a number of constant volume-energy simulations. The closely matched experimental and simulated melting points from these simulations validate the force field for these two compounds.

The glass transition studies performed for myo- and neo-inositol reveal that models consisting of 128 molecules of randomly disordered myo- and neo-inositol molecules, leads to a typical glass transition on heating. The glass transition temperatures calculated for myo-inositol is estimated to be ca. 490 K and for neo-inositol 518 K. Unfortunately, experimentally obtained values are not available; however, the shape of the volume against temperature plots for these two compounds are entirely appropriate for a glass transition.

A comparison of myo- and neo-inositol demonstrates that a very small change in molecular structure leads to a

substantial increase in melting point. Our work is currently ongoing in this area and a forthcoming publication will suggest possible reasons for this.

Another forthcoming publication will compare the bulk structural characteristics of the amorphous models presented in this paper along with other amorphous models prepared from a number of different methods. It is also intended to monitor how these characteristics change as the models approach and pass through the glass transition.

## ACKNOWLEDGMENTS

The authors would like to thank the Pfizer Inc. for financial support and the following people for useful discussions: Dr. James Elliott (Materials Science and Metallurgy, Cambridge University); Dr. Jacco van de Streek (Cambridge Crystallographic Database Center); Dr. Angelo Gavezzotti (Department of Chemistry, University of Milan); Dr. Tony Auffret (Pfizer Global R&D, Sandwich, UK); and Dr. Evgeniy Shalaev (Pfizer Global R&D, Groton, USA).

- <sup>1</sup>S. L. Price, in *Reviews in Computational Chemistry*, Toward More Accurate Model Intermolecular Potentials for Organic Molecules, edited by K. B. Lipkowitz and D. B. Boyd (Wiley, New York, 2002), Vol. 4, Chap. 4, p. 225.
- <sup>2</sup>J. Han, R. H. Gee, and H. Boyd, *Macromolecules* **27**, 7781 (1994).
- <sup>3</sup>M. Tsigis and P. L. Taylor, *Phys. Rev. E* **65**, 021805 (2002).
- <sup>4</sup>E. R. Caffarena and J. R. Grigera, *Carbohydr. Res.* **300**, 51 (1997).
- <sup>5</sup>E. R. Caffarena and J. R. Grigera, *Carbohydr. Res.* **315**, 63 (1999).
- <sup>6</sup>P. B. Conrad and J. J. de Pablo, *J. Phys. Chem. A* **103**, 4043 (1999).
- <sup>7</sup>K. Mazeau and L. Heux, *J. Phys. Chem. B* **107**, 2394 (2003).
- <sup>8</sup>S. Yoshioka, Y. Aso, and S. Kojiman, *Pharm. Res.* **20**, 873 (2003).
- <sup>9</sup>R. West, *Handbook of Chemistry and Physics*, 57th ed. (CRC, Cleveland, Ohio, 1976).
- <sup>10</sup>*Dictionary of Organic Compounds*, 6th ed. (Chapman and Hall, London, 1996), Vol. 4.
- <sup>11</sup>H. Sun, *J. Phys. Chem. B* **102**, 7338 (1998).
- <sup>12</sup>A. R. Leach, *Molecular Modelling: Principles and Applications* (Longman, Harlow, UK, 1996).
- <sup>13</sup>R. D. Andrews, *J. Polym. Sci., Part C: Polym. Symp.* **14**, 261 (1966).
- <sup>14</sup>V. Ferretti, P. Gilli, and A. Gavezzotti, *Chem.-Eur. J.* **8**, 1710 (2002).
- <sup>15</sup>W. L. Jorgensen, D. S. Maxwell, and J. Tirado-Rives, *J. Am. Chem. Soc.* **118**, 11225 (1996).
- <sup>16</sup>J. R. Morris and X. Song, *J. Chem. Phys.* **116**, 9352 (2002).
- <sup>17</sup>Accelrys Ltd, 334 Cambridge Science Park, Cambridge, UK, CB4 0WN.
- <sup>18</sup>F. H. Allen, *Acta Crystallogr., Sect. B: Struct. Sci.* **58**, 380 (2002). The CSD reference codes for myo- and neo-inositol are [MYINOL] and [YEPNOW], respectively.
- <sup>19</sup>Cambridge crystallographic database centre (CCDC), 12 Union road, Cambridge, UK, CB2 1EZ.
- <sup>20</sup>H. J. C. Berendsen, J. P. M. Postma, W. F. van Gunsteren, A. DiNola, and J. R. Haak, *J. Chem. Phys.* **81**, 3684 (1984).
- <sup>21</sup>M. Parrinello and A. Rahman, *J. Appl. Phys.* **52**, 7182 (1981).
- <sup>22</sup>W. C. Swope, H. C. Andersen, P. H. Berens, and K. R. Wilson, *J. Chem. Phys.* **76**, 637 (1982).
- <sup>23</sup>P. W. Atkins, *Physical Chemistry*, 5th ed. (Oxford University Press, Oxford, UK, 1994), p. 200.
- <sup>24</sup>B. C. Hancock and G. Zografi, *J. Pharm. Sci.* **86**, 1 (1997).
- <sup>25</sup>A. Gavezzotti, *Modell. Simul. Mater. Sci. Eng.* **10**, R1 (2002).
- <sup>26</sup>The CSD reference codes for L-chiro-, muco-, and epi-inositol are [FOPKOK], [MUIINOS], and [EPINOS], respectively.